Searching for Millicharged Particles @ $\sqrt{s} = 13.6$ TeV using the MilliQan Detector and Next Generation Forward Physics Detectors

A Progress Update

Presented by Noe Gonzalez

On behalf of the MilliQan Collaboration

University of California Davis

Activities Supervised by Professor Matthew Citron

Abstract:

This paper serves as a documentation of my activities and findings while being in service of the MilliQan experiment's branch at the University of California Davis through the Research Experience for Undergraduates program. While here, my main duties fell into the categories of background analysis and detector commissioning, specifically as they apply to photomultiplier tubes. Key to rejecting large amounts of background in the detector is the calibration of timing systems between the various channels and layers of the MilliQan detector using an understanding of cosmogenic and collision muons. To this end I develop a signature for such particles in the MilliQan detector using known properties of on-board hardware and detector geometry, culminating in the calibration of all internal on-board channels. Additionally, the coming age of the High Luminosity Large Hadron Collider has lead to a push for a new Forward Physics Facility which has spurred the proposal and creation of a variety of specialized detectors. Locally this has been manifested as the ongoing construction of the FORMOSA demonstrator, a new and improved detector to specialize in the search for milli-charged particles produced approximately 500 meters forward of ATLAS giving coverage in the region $|\eta| > 9$ which has been previously unexplored. During the time period of this program I was responsible for characterizing the photomultiplier tubes which will be in use during the lifetime of the FORMOSA demonstrator.

Contents

1 Introduction

On July 4^{th}, 2012 the ATLAS and CMS collaborations at the Large Hadron Collider (LHC), located at CERN, independently announced the discovery of a new boson whose properties were consistent with the hypothesized Higgs boson, having a mass $m_H = 125$ GeV/c^2. Despite this success there have been no new discoveries to suggest physics beyond the standard model (BSM), even though

there are tantalizing hints that suggest there must be. The most apparent is the mere presence of dark matter, a physical reality not accounted for by the Standard Model (SM) of particle physics. Some models (see section 1.1) seek to amend this problem by introducing a Dark Sector (DS) of particles which communicates with SM particles via messengers. If these messengers are massless dark photons, DS particles may have a small SM electromagnetic charge, a millicharge. Unfortunately the general purpose detectors at the LHC, which have access to the largest phase space, suffer from decreased sensitivity due to large hadronic backgrounds and minimum ionization requirements in the calorimeters. MilliQan is a low noise specialty detector comprised of a large scintillating volume (described in more detail in section 2) which allows for the identification of small energy deposits outside of the normal range of experiments like ATLAS and CMS. In order to further minimize backgrounds stemming from detector effects the timing of each on board channel must be precisely calibrated to one another, allowing for quick identification of correlated signals.

A new detector planned to benefit from the increased statistics of the High Luminosity LHC will be placed in the forward region of the ATLAS experiment. This detector, designated as FORMOSA, will serve the same purpose as MilliQan but with updated low noise equipment and a much larger detection volume as well as angular acceptance (see section 4).

1.1 Theory

The Standard Model is best described as a collection of mathematical groups interacting, each group describing a different physical phenomenon. Currently our understanding is summarized by writing the Lagrangian for the theory in the form of these groups, namely

$$\mathcal{L}_{SM} = SU(3) \times SU(2) \times U(1)$$

In this representation $U(1)$ is the group of Electromagnetism, $SU(2)$ is the group of the Weak force, and $SU(3)$ is the group representing the Strong force. Since Dark Matter (DM) is not currently included within the model we can imagine adding a completely new force to this equation by means of a new group. The most logical choice is to choose a group that is both simple and can model DM, namely weak interactions with matter so that observing effects of its presence requires vast amounts. For this reason one introduces a new force described by the group $U^*(1)$, which requires its own mediator (often referred to as the Dark photon) with a coupling proportional to the so-called Dark charge. This is allowed as long as $U^*(1)$ retains the Lorentz invariance of $\mathcal{L}$. However, the inclusion of this new group has a rather interesting result if we include it into the SM representation. The SM Lagrangian is amended and can be rewritten with new cross terms which couple DM and the SM.

$$\mathcal{L} = \mathcal{L}_{SM} - \frac{1}{4} B'_{\mu\nu} B'^{\mu\nu} - \frac{\kappa}{2} B'_{\mu\nu} B^{\mu\nu}$$

Here κ is a kinetic mixing between the SM and Dark $U(1)$ fields with typical values between 10^{-3} and 10^{-2} set by naturalness arguments (effectively $\kappa \sim \alpha/\pi$). The terms B and B' are the electromagnetic and dark sector field tensors. The assumption of $U^*(1)$ group required the introduction of a mediator, the dark photon, but now we make another leap. We assume there exists dark fermions which can feel the effects of dark electromagnetism. One is free to add these fermions into the theory as long as Lorentz invariance is preserved. Applying a gauge transformation to the dark field and defining $B' \to B' - \kappa B$, the Lagrangian becomes

$$\mathcal{L} = \mathcal{L}_{SM} - \frac{1}{4} B'_{\mu\nu} B'^{\mu\nu} + i\bar{\psi}(\partial + i\kappa e' B + ie' B' + iM_{mcp})\psi$$

where the term $-\overline{\psi}\kappa e' B\psi$ is the manifestation of a coupling between some DS fermion and the SM photon in the form of a small charge (which because of the assumed order of κ is often called a milli-charge).

Because of the mixing between the fields, and the subsequent DS fermions with SM charge, any SM electromagnetic process resulting in the creation of oppositely charged particle pairs can instead, through a mixing of the SM photon and DS photon, or a direct SM coupling, create a pair of milli-charged particles (mcp's). One such example is the electromagnetic decay of the SM J/ψ meson (the charm and anti-charm quark bound state) which can proceed as follows.

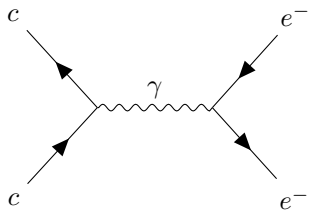

Now, allowing for mixing of the DS and SM one can allow for the following process.

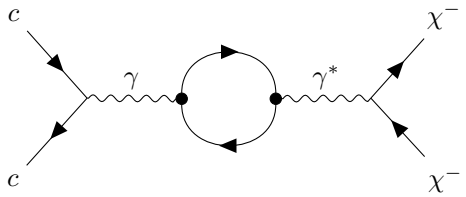

Where χ^- denotes a dark sector mcp and γ^* is the dark photon. Hence, a common phenomena found in *pp* collisions can indeed be key to discovery, provided that the statistics are high enough to observe such an assumed rare occurrence. Oscillations of the photon in Drell-Yan processes (where a quark and anti-quark from separate hadrons interact and annihilate leading to a pair of charged leptons) and Dalitz decays (decay of a meson into a di-lepton pair and a photon) lead to similar production schemes for milli-charged particles.

2 The MilliQan Detector

The search for milli-charged particles is carried out using a 20cm×20 cm×4 m Eljen Ej-200 scintillating volume comprised of 64 inner channels, called bar detectors, and 8 channels in the form of large scintillating detectors, called slabs, arranged such that two are placed on either end of the detector's length, two are placed along the top of the detector, and the remaining four are placed on the sides. A 3D rendering is provided in Figure 1, where the slabs are shown in blue and the tilt of the detector can be seen. MilliQan is inclined in such a way that it is directed towards the CMS interaction point (IP), with the precision alignment being done via laser measurements. Internal to the volume enclosed by the slabs is the set of bar detectors separated into four layers, each layer having 16 bars assembled into a 4×4 grid pattern. All channels are equipped with a photomultiplier tube (PMT) and readout electronics.

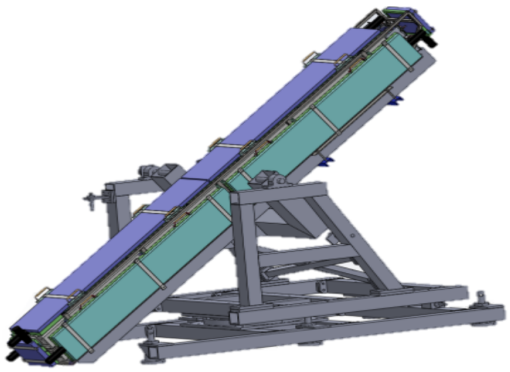

Figure 1: The MilliQan Run3 detector design. The large scintillating detectors placed along the detector length, depicted in light and dark blue, are the so-called slabs used to reject events with cosmic showers.

There are approximately 17m of rock between MilliQan and the CMS IP. MilliQan's detectors are ready to take new data every 2.5 ns which translates to a rate of 0.4 GHz. Pulses within the detector saturate on-board CAEN V1743 digitizers if the output swings to +1.25 V, though this is typically a well known marker of muons because according to the Bethe-Bloch relation,

$$\langle -\frac{dE}{dx} \rangle \propto \frac{Q^2}{m}$$

the muon is minimally ionizing (Q^2/m is small relative to relevant SM background) and hence capable of penetrating the various layers of rock. Each channel is also equipped with reference clocks which can be made to combat thermal emissions of the PMT. These emissions are entirely uncorrelated with every other channel and so can be accounted for by requiring that any pulse

traveling along the length of the detector completes the journey with a speed given roughly by the speed of light.

3 MilliQan Timing Calibration

In order to properly implement a timing calibration, it is essential to establish a physical reference in order to validate the process and find a suitable calibration source. From the Bethe-Bloch relation one can infer that muons are the only suitable SM candidates for calibration. Given their minimally ionizing nature, muons are unlikely to exhaust their kinematic energy when traversing the rock separating the IP and MilliQan, and when they traverse the detector their deposits will be much greater than the signal or background making them clearly distinguishable. Establishing the rest of the muon signature within MilliQan requires proxies for measurements on the particle's energy. Within this experiment the proxies are the max pulse height V_p and the pulse area A_p, where the pulse is integrated over the entire time it is above threshold. The pulse height is less informative as it is limited by the on-board digitizers, so typical values used in the slab and bar detectors are a reflection of this. Pulse area is a reflection of internal characteristics of the scintillating material, its geometry, and the energy of the particle, so it must be sampled for each detector before establishing any threshold.

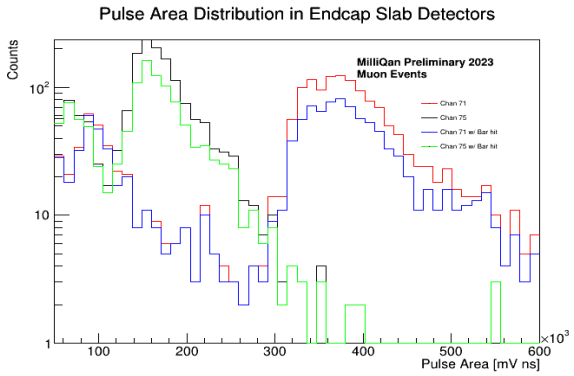

Figure 2: Pulse area distribution for triggering pulses in the slabs located at the ends of the detector (channels 71 and 75). Two cases, with and without requirements on internal pulses, are considered but in general agreement.

Figure 2 shows the distribution of pulse areas in the end cap slab detectors for pulses which saturate in height and are triggering pulses for the same event. For this analysis pulse area cuts of 320 and 150 V ns were used for the downward and upward facing slabs respectively. In order to probe the internal detectors (called bar detectors for their geometry), which join the slabs at the front and

back of MilliQan, they are subjected to a similar pulse area analysis. Only those pulses saturating the bars in height and found to be triggering pulses within a given column are accepted. This allows one to emphasize the signature of cosmic events. The tail end of each distribution is fit using a Gaussian function and the maximum likelihood technique which then gives access to the various saturation values.

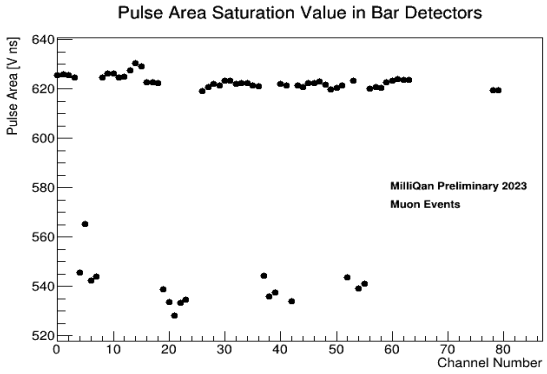

Figure 3: Pulse area distribution for triggering pulses in the bar detectors. There is a clear divide amongst the saturation values which results in the emergence of two populations that must be considered when conducting rigorous analysis.

In Figure 3 the emergence of two populations indicates that global cuts on bar pulse area requirements cannot be made without compromising signal to noise ratios. However, for the purposes of verifying the procedures used in timing calibrations a global pulse area cut of 570 V ns per layer is acceptable. Though this will largely exclude some of the lower saturating channels, pulses from these regions will still be sampled though they will pertain to the upper limits of saturation. Furthermore, the low saturation population makes up a smaller proportion of the inner detectors, meaning that one can effectively analyze the systematic effects of calibration. Tests using lower saturation requirements have been conducted and achieved similar results albeit with worse resolution and larger fitting errors.

In verification, one can estimate the length of detector segments using cosmic and beam muons. If the cuts have been chosen properly and the timing corrections applied to satisfactory precision, then the various layers of channels will act as one. Supposing this is the case, the distribution of timing differences between any two "single" channels (i.e. layers in the case of validating timing calibration) should appear as they would in the end cap slabs with the distance between beam and cosmic muon populations being roughly equal to $2d_{r_j - r_i}/c$ where the subscripts denote that the length d is measured between points r_j and r_i. Applying the aforementioned cuts and using the end cap panels gives a clean measurement of the detector length.

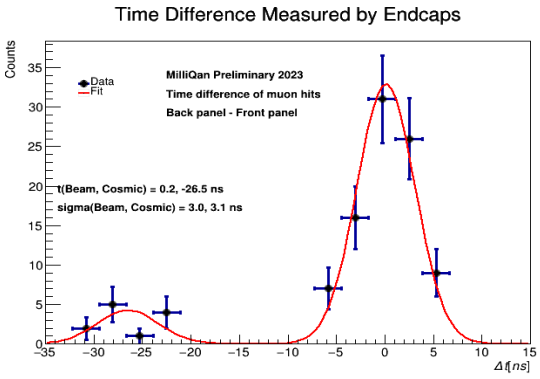

Figure 4: The data is filtered for through going muons using pulse quality requirements and saturation values. Taking the time difference between the end cap slab detectors allows one to build a distribution in which populations of cosmic and beam muons become apparent. Using the time difference between the peaks will allow for a clean measurement of the detector length, which is found to be 3.99±0.12 m and is in agreement with the measured 4.02 m.

The currently measured detector length is 4.02 m and the length as measured with the timing differences is $26.7 \cdot 0.3/2 \approx 3.99 \pm 0.12$ m with the uncertainty being obtained by errors in the fitting of both peaks which were then added in quadrature. This is in good agreement with the measured value and so validates the procedure of checking timing distributions with an easily accessible and measurable quantity. This technique will be used to check all calibrations.

Given that the uncorrelated thermal emissions of a PMT can be overcome by tight timing requirements, all channels require calibration to a reference clock so that particles traveling the speed of light along the length of the detector do so in a recorded time of ∼0 ns. In this way a tight requirement of 15 ns for travel time allows for slower moving particles but is still tight enough to do away with the uncorrelated thermal emissions. The deviations experienced prior to calibration are best exemplified in the figure below where the sudden changes are likely due to external factors such as cable lengths and electronic synchronization with internal factors like individual PMT rise time, which gives way to time walk, giving way to lower contributions. This is because effects of time walk are mostly corrected for by fitting all accepted pulses to a linear model which in turn allows one to counteract delay times.

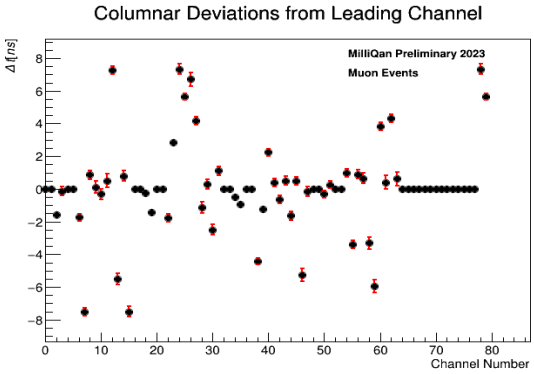

Figure 5: The timing deviation of every channel from its column leader within the 4×4 grid of its respective layer. Deviations for each channel are calculated by fitting a distribution with the maximum likelihood technique.

In Figure 5 the timing deviations are calculated by first building a distribution of Δt's involving the channel of interest and the leading channel of its column within the 4×4 grid of its respective layer. Using a maximum likelihood technique, the distribution of each channel is fit to a Gaussian and the resulting mean, $\overline{\Delta t}$ is used as the channel deviation. Errors are obtained via estimates on the error of relevant fitting parameters. The deviation of each channel defines the negative of a correction constant with respect to the column leader. To calibrate each column of channels to its neighbors within the same layer requires that a suitable path between leading left channels and bottom right channels be selected in order to define an inter-columnar calibration. One is then able to analyze the data for through going muons along the length of the detector to make a measurement of the deviations between layers. Using layer 0, the set of bars closest to the CMS IP, as the reference clock a new correction at the layer level is defined to set all incoming beam muons to have a registered time difference of ~ 0 ns.

The Δt distribution between the first layer and final layer of bar detectors is presented in Figure 6. Calculation of the distance preceded in the same manner as in section 3.1 and uncertainties were determined by adding in quadrature the errors on the means of each peak, which were obtained using a maximum likelihood technique. The estimate of the distance between the first and last layers is reported as 2.44 ± 0.13 m which is in agreement with the currently measured value of 2.58m.

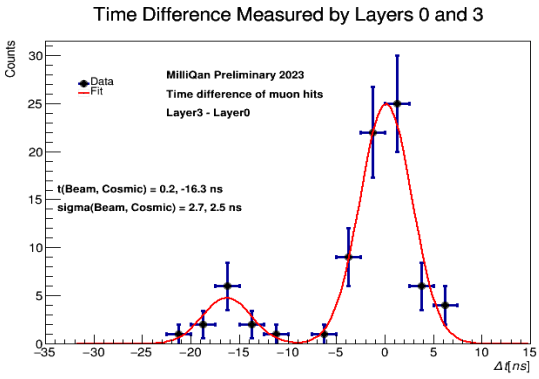

Figure 6: Time differences for incoming cosmic and beam muons taken by using the recorded time stamps in the first and last layers of bar detectors. Using the difference between the two peaks the distance is estimated at 2.44 ± 0.13 m while the measured value is 2.58m.

All channels associated with a bar detector are then calibrated to the lowest facing slab detector, completing the synchronization and allowing for one to use any part of the detector for clean measurements of the various detector regions and estimates on particle traversal time. With the calibration constants obtained the MilliQan offline data analysis is one step closer to commencement, with plans to have an initial analysis begin roughly at the end of this year.

4 FORMOSA at UC Davis

With the high luminosity Large Hadron Collider estimated to begin physics operations in the year 2029, efforts to make use of every collision have increased greatly. The center of mass energy and luminosity increases will bring about the best chances to discover new and exciting physics, but the general detectors like CMS and ATLAS will be helpless to detect everything. Though extremely precise and covering large areas, CMS and ATLAS are not sensitive enough to discover micro-charged particles, and they only cover a finite region extending from $-5 < \eta < 5$. However, current efforts to introduce a new Forward Physics Facility at ATLAS will allow coverage in the $9 < |\eta|$ regions using specialty detectors constructed by smaller scale collaborations. The Forward Micro-Charge Search experiment, or FORMOSA as it is called, will be one such specialty detector with a focus on the search for fractionally charged particles which are consistent with the predictions of dark matter introduced as a $U(1)$ group. This experiment will act as much more sensitive extension of MilliQan with the expectation for access to many more statistics due to its location and relative solid angle coverage. In order to increase sensitivity and statistics at the forward region FORMOSA requires a large detector area facing the ATLAS

IP and low noise design to reduce possible backgrounds. Because the Forward Physics Facility will be located outside of the ATLAS cavern, SM backgrounds are attenuated in a similar fashion to MilliQan, which leaves electronic noise as the greatest adversity.

While FORMOSA will be equipped with an updated photomultiplier tube (though again supplied by Hamamatsu), the essential physics leading to noise is the same and must be well characterized since it is this background which will lead to energy calibrations one can use to further reject backgrounds and extract signals.

4.1 Electronic Calibrations

FORMOSA will be utilizing R7725 photomultiplier tubes from Hamamatsu in order to amplify signals produced by high energy particles traveling through scintillator material (Eljen Ej-200) which will make up the bulk of FORMOSA's body. Photomultiplier tubes in general consist of a large photocathode and several secondary electrodes referred to as dynodes. It is the large photocathode in combination with the scintillator which are responsible for generating the primary electron, via the photoelectric effect, which is then multiplied by subsequent collisions with the dynodes whose position, shape, and material structure are manufactured precisely to match the geometry of the photocathode, the expected field gradient, and desired gain (which varies with applied bias). The issue with this scheme is that although a proper (that is to say, generated by an interaction of light with the photocathode) primary electron will generate a pulse constituted of 10^6 electrons, primary electrons from the photocathode are also generated by thermal emission of electrons which proceeds identically to the photoelectric effect but with the source of energy being due to thermal fluctuations. The result is a lower energy primary electron still capable of producing thousands, if not more, secondary electrons which will be read in as a pulse. The inability to distinguish between this thermal emission process (dark current as it is sometimes called; or dark rate if measuring the output frequency rather than current) and actual events generated from scintillator activity would be catastrophic. One the one hand, these dark currents can be eliminated from the signal with tight timing cuts, as they are in MilliQan, but this relies on the emission rates being uncorrelated. For very rare signals, which is expected for mcps, even a few falsely correlated emissions over the course of many data taking sessions may mean the difference between finding new physics and excluding the wrong regions of phase space. Having a good estimate of detector efficiency, dark rates, and the amplitude of signals originating from a single photoelectron allow one to effectively characterize the particle which created the scintillation photon and estimate the total number of events which are due to correlated thermal emissions.

The first challenge we confronted at UC Davis was transforming the newly obtained rooms into proper testing facilities with suitable equipment. This meant that we had to remove most computers, monitors, microphones, extra seats, and trash from the old conference room and designate a bench for PMT

testing which was suitably close to the data acquisition electronics, power supply voltage and outlets. Once this was done it became necessary to construct a dark box which was a doubly layered cardboard box with each layer completely covered in a thick dark tape to prevent light from interacting with the PMT photocathode during dark current testing. Additional precautions were taken by temporarily covering the windows with a sheet of cardboard after closing the exterior blinds. After this had been done proper handling required a temporary break period in which cotton and latex gloves were ordered to prevent the contamination of the photomultiplier tubes glass exterior. A protective covering of tyvek (reflective material) and thick dark paper were wrapped around the exterior of each tube prior to testing in order to prevent stray photons from any possible cracks in the box, while also preventing possible oil contamination from handling. Testing procedures further dictated that prior to data taking the PMT must be rested, i.e. no bias applied, in a light tight environment for a minimum of 30 minutes.

Figure 7: The FORMOSA PMT testing dark box. A doubly layered cardboard arrangement with thick tape covering all external surfaces of each layer. Can comfortably accommodate a 1m x 5cm scintillator bar with PMT pressed up against it.

The dark box utilized by the UC Davis group is shown in Figure 7 where the power supply (CAEN power supply in red and grey) and DRS oscilloscope (small grey box with a yellow label on it and SMA cable attached to one of its ports) are viewable in the rightmost background. Although it was possible to take initial dark current data, results were not consistent with those from UC Santa Barbara (a collaborator in the experiment). In order to diagnose the

problem the PMT tested by our group and UC Santa Barbara were re-tested at the UC Davis laboratory in which the results indicated a result in line with the previous test conducted by UC Davis. Understanding the issue required firstly a check on the PMT quality to ensure no component had been damaged which can be conducted by analyzing the response of each device. Of particular interest was the logarithm of bias voltage and the logarithm of the resulting mean pulse area of each signal since these are expected to be directly proportional to each other.

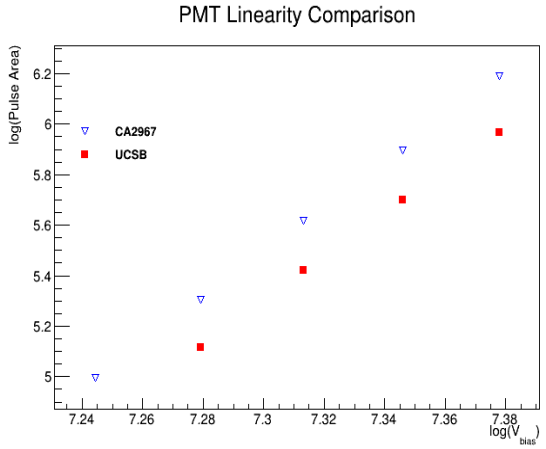

Figure 8: A comparison of PMT quality variables between one received and tested at UC Davis with another on loan from UC Santa Barbara. The results indicate no abnormality.

Analysis of the results in Figure 8 indicated no abnormality and in fact pointed to good health. Several other variables were scrutinized such as the monitor brightness, stress on both the data acquisition and power supply cables, light leaks, and contact of the PMT's with the interior of the dark box. Unfortunately the construction of the testing environment made it difficult to decouple the various factors so a systematic deconstruction of the environment was necessary, beginning with the material in immediate contact with the PMT. Since there was no good agreement on what the correct dark current should be, trouble shooting the testing setup required a new approach. Instead, measurements of the mean pulse area resulting from an interaction of Cd-109 and a scintillator bar were used since the result was expected to always be well removed from the noise level, which is the pulse area from thermally emitted electrons sometimes called the SPE peak (SPE for single photoelectron since thermal emission practically guarantees that a single electron is liberated from the photocathode). To further reduce the possibility that these measurements would not be affected by potentially faulty PMT's, a new one was selected to be representative of the minimally handled group.

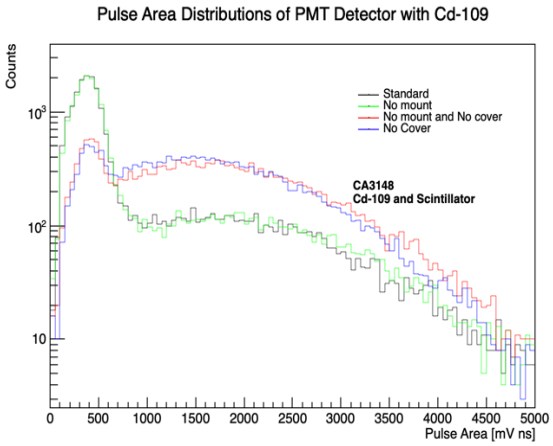

Figure 9: Pulse area distribution for different levels of direct contact with the PMT. The Cd-109 peak is non-existent for the maximal contact (standard) case and when the mount connecting the PMT and scintillator is removed. Results indicate that the wrapping of tyvek and black paper introduced for handling precautions were lead contributors to the issues being faced.

The following configurations were tested.

1. Standard - 3D mount connecting the PMT and Scintillator bar, tyvek and black paper wrapping on the PMT, all covered by the dark box.
2. No mount - Same as standard with the 3D mount removed. In this case the PMT was pressed carefully against the face of the scintillator and precautions for minimal movement post positioning were taken.
3. No mount and no cover - Same as no mount with the addition of removing the wrapping of tyvek and black paper.
4. No cover - Same as standard with the removal of tyvek and black paper.

Examining the distributions in Figure 9 shows that the largest contributor to the vanishing of the Cd-109 peak was direct contact with the glass container of the photomultiplier tube. Investigating the dark rate reveals the same conclusion (though the rates are inflated because of the decay process of Cd-109). Since this test, further developments were made to reduce contact with the devices and dark rates have greatly reduced, even reaching tens of Hz compared to the initial values of approximately 3.5 KHz.

5 Conclusion

The MilliQan and FORMOSA experiments are a new generation of low noise scintillator based detectors which aim to test the hypothesis of milli(micro)-

charged particles which are beyond the sensitivity of experiments like CMS. Although FORMOSA will not be constructed for a while, its demonstrator (which is essentially a quarter of the detector) has work underway and calibrations of the photomultiplier tubes used in this demonstrator were conducted during my visit. However, my primary work was establishing a proper testing procedure and environment which would allow accurate measurements of the dark currents and thus estimates of background in analyses conducted when it is in operation. The MilliQan experiment has been taking data during Run 3 of the LHC and this summer I conducted timing calibrations while more work was conducted to check data quality prior to the start of data analysis scheduled to begin later this year. With the work completed this summer, FORMOSA and MilliQan are prepared to investigate never before accessed regions of phase space to test proposed dark sector hypotheses.

6 References

1. Anchordoqui, et al.The Forward Physics Facility: Sites, Experiments, and Physics Potential.May 2022.arXiv:2109.10905v2 [hep-ph]

2. Hamamatsu Photonics. PHOTOMULTIPLIER TUBES Basics and Applications. Fourth Edition. 2017. Hamamatsu Photonics K.K.

3. MilliQan Collaboration.Search for millicharged particles in proton-proton collisions at $\sqrt{s} = 13$ TeV.May 2020.arXiv:2005.06518 [hep-ex]

4. MilliQan Collaboration.Sensitivity to millicharged particles in future proton-proton collisions at the LHC.April 2021.arXiv:2104.07151 [hep-ex]